
A ROBUST MIXED-EFFECTS QUANTILE REGRESSION MODEL USING GENERALIZED LAPLACE MIXTURES TO HANDLE OUTLIERS AND SKEWNESS

Divan A. Burger

Syneos Health, Bloemfontein, Free State,
South Africa

Department of Mathematical Statistics and Actuarial Science, University of the Free State, Bloemfontein,
South Africa
divanaburger@gmail.com

Sean van der Merwe

Department of Mathematical Statistics and Actuarial Science, University of the Free State, Bloemfontein,
South Africa

Emmanuel Lesaffre

I-BioStat, KU Leuven, Leuven,
Belgium

Department of Statistics and Actuarial Science, University of Stellenbosch,
South Africa

April 22, 2025

ABSTRACT

Mixed-effects quantile regression models are widely used to capture heterogeneous responses in hierarchically structured data. The asymmetric Laplace (AL) distribution has traditionally served as the basis for quantile regression; however, its fixed skewness limits flexibility and renders it sensitive to outliers. In contrast, the generalized asymmetric Laplace (GAL) distribution enables more flexible modeling of skewness and heavy-tailed behavior, yet it remains vulnerable to extreme observations. In this paper, we extend the GAL distribution by introducing a contaminated GAL (cGAL) mixture model that incorporates a scale-inflated component to mitigate the impact of outliers without requiring explicit outlier identification or deletion. We apply this model within a Bayesian mixed-effects quantile regression framework to model HIV viral load decay over time. Our results demonstrate that the cGAL-based model more reliably captures the dynamics of HIV viral load decay, yielding more accurate parameter estimates compared to both AL and GAL approaches. Model diagnostics and comparison statistics confirm the cGAL model as the preferred choice. A simulation study further shows that the cGAL model is more robust to outliers than the GAL and exhibits favorable frequentist properties.

1 Introduction

Mixed-effects quantile regression models have become increasingly important in statistical analyses because they account for the correlation structure inherent in repeated or clustered measurements, thus facilitating more accurate inference of the conditional distribution across various quantiles [1, 2]. Under a standard mixed-effects framework, this approach is well-suited to heteroscedastic settings, where variability can differ substantially across individuals or groups. In longitudinal clinical trials, for example, certain treatments may have a stronger effect on patients in the lower or upper tails of the response distribution than those near the mean. By capturing these diverse responses, quantile-based methods reveal treatment effects that mean-focused analyses might overlook. The asymmetric Laplace (AL) distribution has long been the favored choice for parametric mixed-effects quantile regression because its fixed skewness parameter directly targets the quantile of interest [2].

Despite its usefulness, the AL distribution in quantile regression has a key limitation: its skewness parameter is locked to a specific quantile. Rather than estimating skewness, one must pre-select it based on the quantile of interest. For instance, modeling the 25th quantile (Q25) necessitates a right-skewed AL distribution, and this skewness grows more pronounced for lower quantiles, such as the 10th percentile. Consequently, if the actual data shape deviates from the skewness imposed by the AL distribution, the model may simply provide a poor fit.

To overcome the AL distribution’s forced skewness constraint, Yan and Kottas [3] proposed the generalized AL (GAL) distribution, which gives greater flexibility for asymmetric and heavy-tailed data. Yu and Yu [4] further extended this approach to mixed-effects models in a quantile regression framework. By adding an estimable shape parameter, the GAL distribution accommodates a wider range of skewness and kurtosis, making it more adaptable than the AL in many settings.

However, while the GAL distribution is more flexible, it can still be vulnerable to extreme outliers, especially in heavy-tailed data. By construction, its location parameter is the p_0 th quantile. When p_0 is close to 0.5, both tails remain relatively heavy. But as p_0 moves away from 0.5 (i.e., $p_0 \rightarrow 0^+$ or $p_0 \rightarrow 1^-$), the skewness parameter “lightens” one tail while weighting the other more heavily, leaving the lighter-tail side more susceptible to outliers. To address this, we propose a more robust approach: the contaminated GAL (cGAL) distribution. Constructed as a mixture of two GAL components, the cGAL inflates the variance of the second component to account for extreme observations, effectively mitigating outlier sensitivity. Crucially, it retains the property that the location parameter aligns with the targeted quantile, preserving interpretability while reducing sensitivity to skewness and outliers.

Other relevant work includes Barata [5], which examined dynamic quantile regression using the GAL distribution in Bayesian settings, though without extending it to mixed models or multivariate data with cluster-level random effects. Florez et al. [6] applied quantile regression to multivariate and longitudinal data with the multivariate generalized hyperbolic distribution, which effectively models complex dependence but omits random effects and relies on the Bessel function, complicating computation. Wichitaksorn et al. [7] explored flexible Bayesian quantile regression via scale mixtures of truncated normals. However, akin to AL, their methods lack asymmetry at middle quantiles and produce lighter tails at extremes, increasing outlier sensitivity. Moreover, these approaches do not extend to random effects. Bernardi et al. [8] employed the skew exponential power distribution for quantile regression, yielding more flexible tails than the AL but applying it only to fixed-effects models, thus excluding random and mixed model contexts.

In this paper, we adopt a Bayesian approach to estimate parameters of the mixed-effects cGAL model with JAGS [9]. This approach enables full posterior inference and does not rely on asymptotic approximations. Full posterior inference can be especially beneficial for smaller or more complex models. Because JAGS supports flexible, user-defined model specifications, our conceptual approach can be translated directly into code, which conveniently facilitates the implementation of the proposed mixed-effects quantile regression model.

We apply the proposed model to a human immunodeficiency virus (HIV) viral load dataset, using a nonlinear mixed-effects (NLME) model to capture patient-specific trajectories of viral load decay across various quantiles.

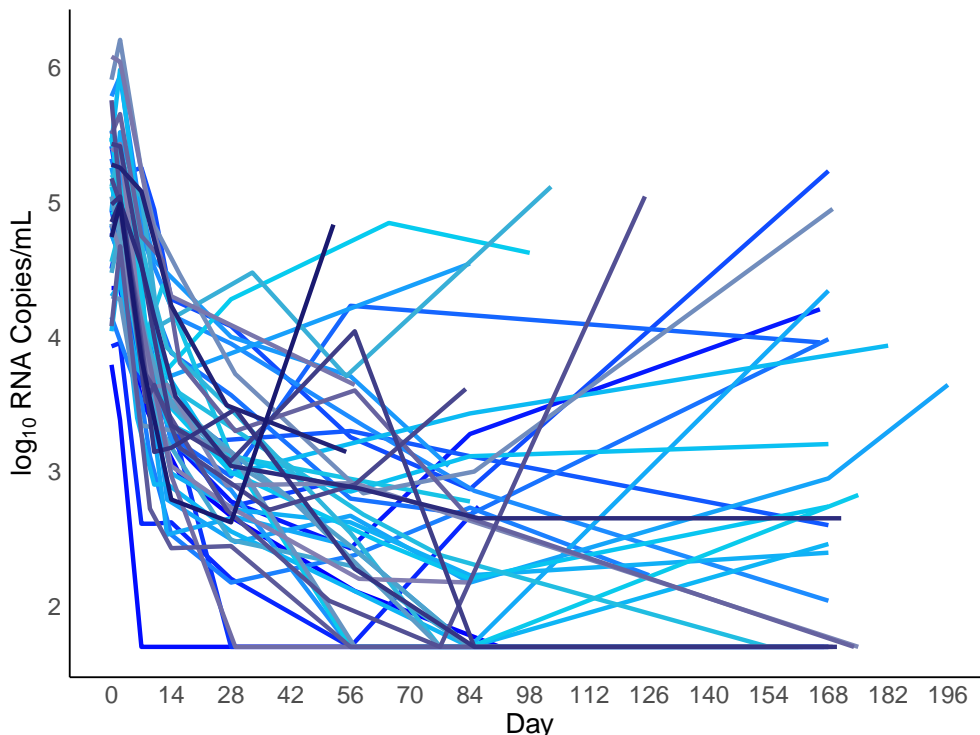


Figure 1: HIV viral load over time among patients in the ACTG 315 study. Each line shows an individual patient’s \log_{10} HIV viral load.

The remainder of this paper is organized as follows: Section 2 describes the ACTG 315 HIV clinical trial dataset that motivates our analysis. In Section 3, we present the quantile regression distributions used (AL, GAL, and cGAL). Section 4 outlines the Bayesian mixed-effects model for quantile regression. Section 5 applies these methods to the HIV dataset to demonstrate their use in a real-world context. In Section 6, we conduct a simulation study by sampling from the cGAL model and then fitting cGAL and GAL models to compare their performance under varying degrees of contamination and assess their sensitivity to outliers. Finally, Section 7 presents concluding remarks and outlines possible directions for future research.

2 ACTG 315 HIV clinical trial

The ACTG 315 dataset, available in the `ushr` package in R [10], includes longitudinal measurements of HIV viral load (\log_{10} RNA copies/mL) over time. It features data on 46 patients, with the longest measurement recorded on Day 196 after baseline (Day 0). Models of HIV viral load dynamics typically show a biphasic decline: an initial rapid reduction in viral load due to effective antiretroviral therapy, followed by a slower stabilization phase as the virus is further suppressed [11]. Traditionally, many analyses (e.g., generalized linear models) have concentrated on the mean response, giving insights into average patient trajectories. Yet such approaches often overlook the considerable variability among patients, as shown in Figure 1. Some patients experience sharper declines, while others have irregular fluctuations or slower viral suppression, indicating outliers or subgroups with distinct response patterns [12]. A more flexible framework, such as quantile regression, is therefore needed to capture the full distribution of viral load trajectories and better understand HIV progression across diverse patient subgroups.

We use an NLME quantile regression model that accounts for both the nonlinear dynamics of viral load and the presence of outliers, such as biologically extreme surges or measurement errors. In particular, we apply the cGAL model, which

extends the GAL distribution through a contamination mechanism to address irregularities in typical viral load data. By comparing the cGAL model with the standard GAL model, we demonstrate that a robust quantile regression approach can yield more reliable predictions and insights into HIV progression, especially in the presence of outliers.

3 Laplace distributions for quantile regression

This section introduces the three Laplace distributions used in quantile regression in this paper: the AL distribution, the GAL distribution, and its robust extension, the cGAL distribution.

3.1 Asymmetric Laplace distribution

Consider a random variable $y \in \mathbb{R}$ following the AL distribution. The probability density function (PDF) of the AL distribution is given by:

$$f_{\text{AL}}(y|\mu, \sigma, p_0) = \frac{p_0(1-p_0)}{\sigma} \exp\left\{-\rho_{p_0}\left(\frac{y-\mu}{\sigma}\right)\right\},$$

where $\mu \in \mathbb{R}$ is a location parameter, representing the p_0^{th} quantile, $\sigma > 0$ is a scale parameter, and $p_0 \in (0, 1)$ is a skewness (quantile) parameter, fixed *a priori* (e.g., 0.25 for the first quartile). When $p_0 = 0.5$, the distribution is symmetric around μ , corresponding to the standard Laplace distribution. The distribution is skewed for $p_0 \neq 0.5$, with skewness increasing as p_0 moves away from 0.5.

The function $\rho_{p_0}(u)$ is defined as:

$$\rho_{p_0}(u) = u(p_0 - \mathbf{1}(u < 0)),$$

where the indicator function $\mathbf{1}(u < 0)$ is defined as:

$$\mathbf{1}(u < 0) = \begin{cases} 1, & \text{if } u < 0, \\ 0, & \text{if } u \geq 0. \end{cases}$$

The piecewise function $\rho_{p_0}(u)$ governs the exponential decay on either side of μ , with asymmetry controlled by p_0 . In quantile regression, p_0 thus specifies the distribution's focus (e.g., the 25th vs. 75th quantile).

By construction, μ satisfies:

$$\int_{-\infty}^{\mu} f_{\text{AL}}(y|\mu, \sigma, p_0) dy = p_0,$$

confirming μ as the p_0^{th} quantile.

The AL distribution can also be viewed as a normal-exponential mixture:

$$f_{\text{AL}}(y|\mu, \sigma, p_0) = \int_0^{\infty} \mathcal{N}(y|\mu + \theta_1 z, \sigma^2 \theta_2^2 z) \text{Exp}(z|1) dz, \quad (1)$$

where $\mathcal{N}(y|\mu_N, \sigma_N^2)$ denotes the normal distribution with mean μ_N and variance σ_N^2 , and $\text{Exp}(z|1)$ is the exponential distribution with rate 1. The parameters θ_1 and θ_2^2 are functions of p_0 and are given by:

$$\theta_1 = \frac{1-2p_0}{p_0(1-p_0)}, \quad \theta_2^2 = \frac{2}{p_0(1-p_0)}.$$

The AL distribution is commonly used in quantile regression because its skewness parameter p_0 directly targets a chosen quantile. However, while its tails are heavier than the normal distribution (the standard Laplace has kurtosis 6), it can still be sensitive to very heavy-tailed or extreme observations, prompting the need for more flexible alternatives such as the GAL and cGAL distributions. These extensions are explored next.

3.2 Generalized asymmetric Laplace distribution

Next, consider the GAL distribution suggested by Yan and Kottas [3], which generalizes the AL. As with the AL distribution, we fix μ to be the p_0^{th} quantile so that

$$\int_{-\infty}^{\mu} f_{\text{GAL}}(y|\mu, \sigma, \gamma, p_0) dy = p_0,$$

where $\sigma > 0$ and $\gamma \neq 0$ control the scale and shape around the p_0^{th} quantile μ . We then standardize y by defining

$$y^* = \frac{y - \mu}{\sigma}.$$

Next, define the terms:

$$p_{\gamma^+} = p - \mathbf{1}(\gamma > 0), \quad p_{\gamma^-} = p - \mathbf{1}(\gamma < 0),$$

$$g(\gamma) = 2\Phi(-|\gamma|) \exp\left(\frac{\gamma^2}{2}\right), \quad p \equiv p(\gamma, p_0) = \mathbf{1}(\gamma < 0) + \left\{ \frac{p_0 - \mathbf{1}(\gamma < 0)}{g(\gamma)} \right\},$$

where $\Phi(\cdot)$ is the standard normal cumulative distribution function (CDF), and γ lies in the interval (L_γ, U_γ) , defined by roots of $g(\gamma) = 1 - p_0$ and $g(\gamma) = p_0$.

For $\gamma \neq 0$, the GAL PDF is:

$$f_{\text{GAL}}(y|\mu, \sigma, \gamma, p_0) = \frac{2p(1-p)}{\sigma} \left[\left(\Phi\left(\frac{-p_{\gamma^+}y^*}{|\gamma|} + \frac{p_{\gamma^-}}{p_{\gamma^+}}|\gamma|\right) - \Phi\left(\frac{p_{\gamma^-}}{p_{\gamma^+}}|\gamma|\right) \right) \exp\left\{-p_{\gamma^-}y^* + \frac{\gamma^2}{2}\left(\frac{p_{\gamma^-}}{p_{\gamma^+}}\right)^2\right\} \mathbf{1}\left(\frac{y^*}{\gamma} > 0\right) + \exp\left\{-p_{\gamma^+}y^* + \frac{\gamma^2}{2}\right\} \Phi\left(-|\gamma| + \frac{p_{\gamma^+}y^*}{|\gamma|} \mathbf{1}\left(\frac{y^*}{\gamma} > 0\right)\right) \right],$$

which reduces to the AL distribution when $\gamma \rightarrow 0$.

The GAL distribution can also be expressed as a triple mixture of normal, exponential, and truncated normal variables:

$$f_{\text{GAL}}(y|\mu, \sigma, \gamma, p_0) = \int_0^\infty \int_0^\infty \mathcal{N}(y|\mu + \sigma C|\gamma|s + \sigma A z, \sigma^2 B z) \text{Exp}(z|1) \mathcal{N}^+(s|0, 1) dz ds, \quad (2)$$

where $\mathcal{N}^+(s|0, 1)$ is a truncated normal on the positive real line, and

$$A \equiv A(p) = \frac{1-2p}{p(1-p)}, \quad B \equiv B(p) = \frac{2}{p(1-p)}, \quad C \equiv C(\gamma, p) = [\mathbf{1}\{\gamma > 0\} - p]^{-1}.$$

While the GAL distribution presents greater flexibility in modeling skewness and accommodating heavier tails compared to the AL, as will be demonstrated in the next section, its kurtosis is capped, limiting its ability to capture extremely heavy-tailed behavior.

3.3 Contaminated generalized asymmetric Laplace distribution

To increase the robustness of a quantile model to outlying values, we introduce the cGAL distribution, formed as a mixture of two GAL distributions. Both components share the same location μ but differ in scale parameters: σ for the main component and $\tau_0\sigma$ for the ‘‘contaminated’’ component, where $\tau_0 > 1$. Let $\alpha \in (0, 1)$ be the mixture weight. The cGAL PDF is:

$$f_{\text{cGAL}}(y|\mu, \sigma, \gamma, \alpha, p_0) = (1 - \alpha) f_{\text{GAL}}(y|\mu, \sigma, \gamma, p_0) + \alpha f_{\text{GAL}}(y|\mu, \tau_0\sigma, \gamma, p_0).$$

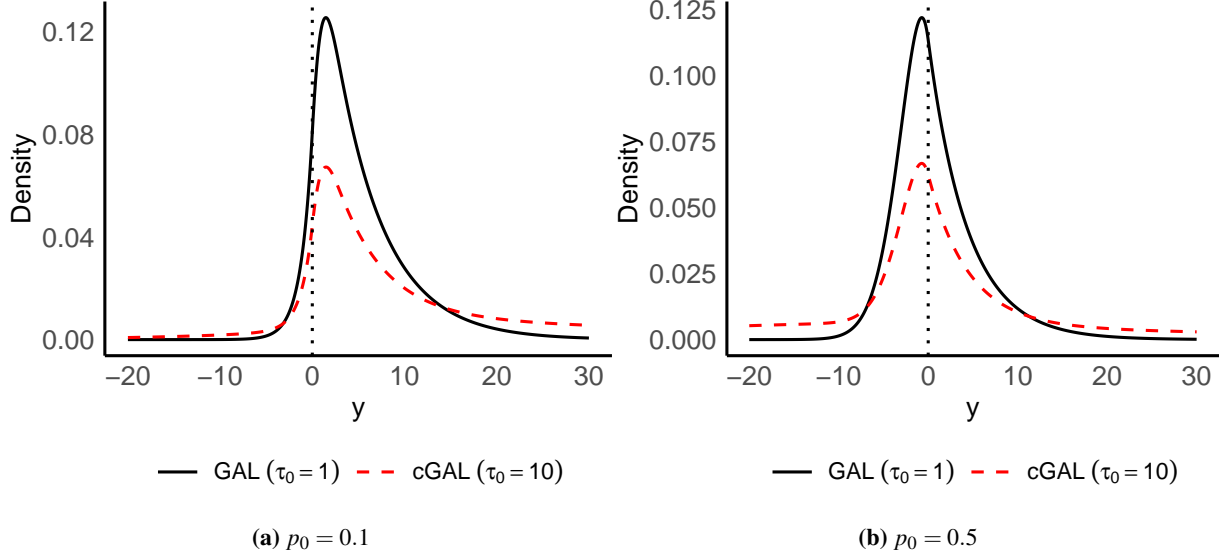


Figure 2: PDF comparison of GAL and cGAL distributions for $p_0 = 0.1$ with $\gamma = 1$ and $p_0 = 0.5$ with $\gamma = -0.625$, assuming $\mu = 0$ and $\sigma = 1$. The cGAL distribution is shown for $\tau_0 = 10$ and $\alpha = 0.5$, while the GAL corresponds to $\tau_0 = 1$. When $\tau_0 > 1$ and $\alpha \neq 0, 1$, cGAL exhibits heavier tails, making it more robust to outliers. The black dotted line at $y = 0$ indicates the p_0^{th} quantile.

By inflating the scale in the second component, the cGAL distribution can better accommodate outliers. This two-component, scale-inflated mixture approach closely resembles the well-known contaminated normal distribution [13, 14].

Because each component has the same location μ , the mixture preserves μ as the p_0^{th} quantile:

$$F_{\text{cGAL}}(y|\mu, \sigma, \gamma, \alpha, p_0) = (1 - \alpha) F_{\text{GAL}}(y|\mu, \sigma, \gamma, p_0) + \alpha F_{\text{GAL}}(y|\mu, \tau_0\sigma, \gamma, p_0),$$

where $F_{\text{GAL}}(y|\mu, \sigma, \gamma, p_0)$ is the CDF of the GAL distribution with parameters μ , σ , γ , and p_0 . Evaluating at $y = \mu$ yields $F_{\text{cGAL}}(\mu) = p_0$. The parameter α controls the contamination degree: as $\alpha \rightarrow 0$, the model reverts to the standard GAL distribution; as $\alpha \rightarrow 1$, it degenerates to a single, inflated-scale GAL (with scale $\tau_0\sigma$), and is thus no longer a two-component contaminated distribution. Larger values of τ_0 inflate the tails more strongly, improving robustness against extreme outliers.

Figure 2 compares the PDFs for the GAL and cGAL distributions at two quantiles, $p_0 = 0.1$ with $\gamma = 1$ and $p_0 = 0.5$ with $\gamma = -0.625$, assuming $\mu = 0$ and $\sigma = 1$. The cGAL distribution, shown for $\tau_0 = 10$ and $\alpha = 0.5$, exhibits heavier tails compared to the GAL distribution ($\tau_0 = 1$) when contamination occurs.

Figure 3 presents the sample kurtosis and skewness for the GAL and cGAL ($\tau_0 = 10$, $\alpha = 0.5$) distributions as functions of the parameter γ to illustrate the impact of contamination in the cGAL distribution on both the tails and asymmetry of the distribution in comparison to the GAL model for two quantiles ($p_0 \in \{0.1, 0.5\}$). The left and right L-statistic kurtosis [15] are displayed alongside both distributions' overall kurtosis and skewness. Details on the calculation of the L-statistic kurtosis can be found in Appendix A. For instance, the GAL distribution exhibits lighter-than-normal left tails at the lower decile ($p_0 = 0.1$). However, with the introduction of contamination in the cGAL distribution, the left tail becomes heavier, making it more robust to outliers, particularly for modeling at the lower decile ($p_0 = 0.1$).

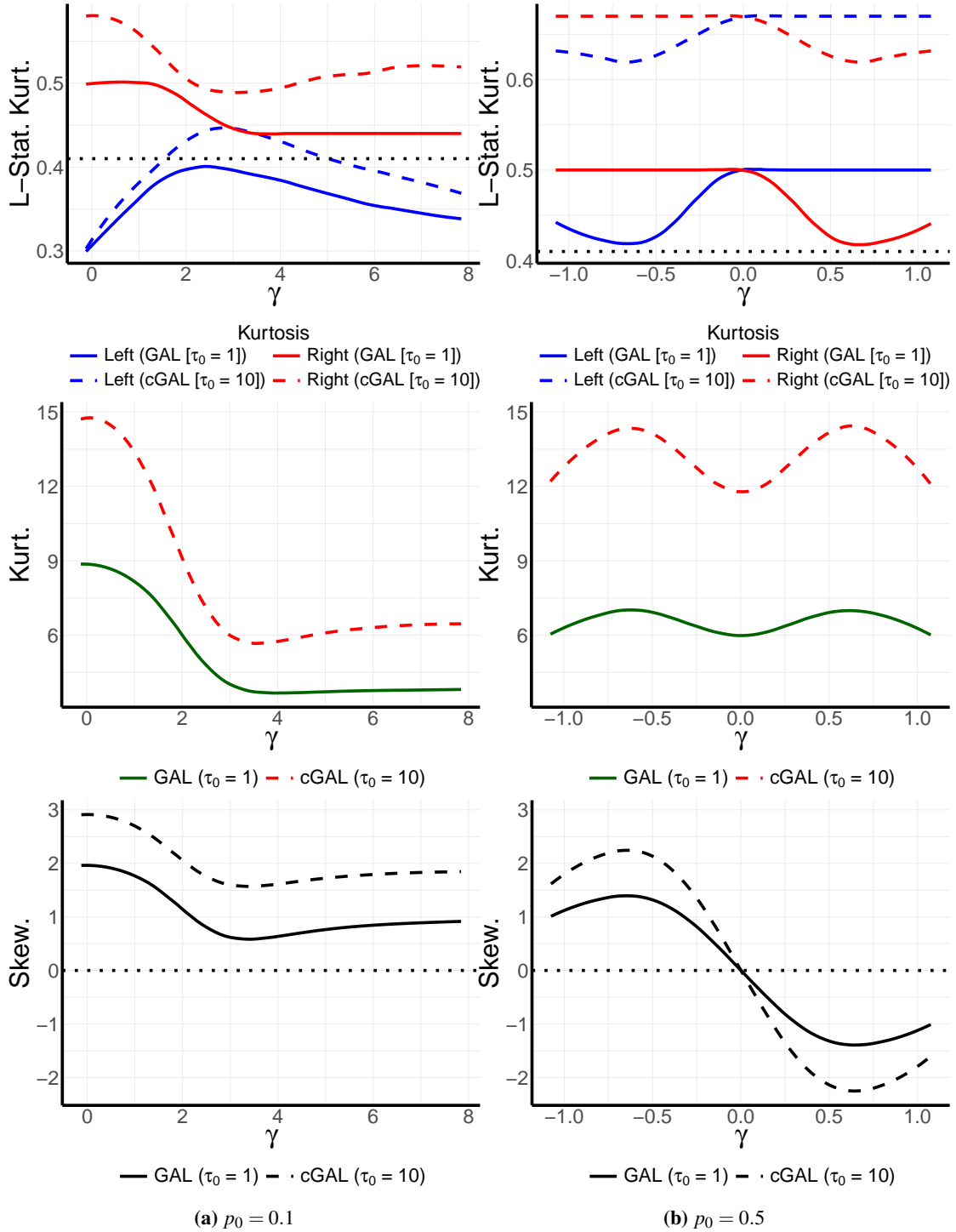


Figure 3: Kurtosis and skewness for GAL and cGAL ($\tau_0 = 10$, $\alpha = 0.5$) over γ . Left and right L-statistic kurtosis [15] are shown in blue and red, respectively. A dotted black line marks the normal-reference kurtosis of 0.4142. The overall kurtosis (green) and skewness (black) for GAL ($\tau_0 = 1$, solid) vs. cGAL ($\tau_0 = 10$, dashed) highlight cGAL's heavier tails and increased robustness. A dotted line at 0 on the skewness plot indicates symmetry.

4 Bayesian mixed-effects quantile regression model

This section outlines the general form of this study’s mixed-effects quantile regression model and its Bayesian specification. We now embed the AL, GAL, and cGAL distributions into a hierarchical framework for repeated measures or clustered data.

Let y_{ij} denote the response variable for subject or cluster i ($i = 1, \dots, N$) and observation j ($j = 1, \dots, J_i$). We model y_{ij} as:

$$y_{ij} = \mu_{ij}(p_0) + \varepsilon_{ij}(p_0),$$

where $\mu_{ij}(p_0)$ is the conditional p_0^{th} quantile of y_{ij} given the covariates and $\varepsilon_{ij}(p_0)$ is the error term such that the p_0^{th} quantile of $\varepsilon_{ij}(p_0)$ is zero. Thus, the distribution of $\varepsilon_{ij}(p_0)$ is centered at zero in the “ τ -quantile” sense.

The quantile $\mu_{ij}(p_0)$ conditional on random effects is modeled as a function of fixed effects, random effects, and covariates:

$$\mu_{ij}(p_0) = g(\mathbf{x}_{ij}, \boldsymbol{\beta}, \mathbf{b}_i),$$

with \mathbf{x}_{ij} being the vector of covariates for observation j of subject i , $\boldsymbol{\beta}$ the vector of unknown fixed-effect parameters, $\mathbf{b}_i \in \mathbb{R}^d$ the vector of random effects for subject i , and g a known link function, which can be linear or nonlinear (e.g., a compartmental viral load decay model).

The random effects \mathbf{b}_i are assumed to follow a multivariate normal distribution with mean $\mathbf{0}$ and covariance matrix $\boldsymbol{\Sigma}$:

$$\mathbf{b}_i \sim \text{MVN}(\mathbf{0}, \boldsymbol{\Sigma}). \quad (3)$$

The mixed-effects quantile model is formulated under the three different distributional frameworks in Section 3: the AL, GAL, and cGAL distributions. In the AL model, y_{ij} follows $f_{\text{AL}}(y_{ij} | \mu_{ij}(p_0), \sigma, p_0)$. The GAL model introduces a skewness parameter, giving $f_{\text{GAL}}(y_{ij} | \mu_{ij}(p_0), \sigma, \gamma, p_0)$. Lastly, the cGAL model incorporates an additional contamination parameter to handle outliers, leading to $f_{\text{cGAL}}(y_{ij} | \mu_{ij}(p_0), \sigma, \gamma, \alpha, p_0)$.

In the cGAL setting, “outliers” or extreme data points are partially explained by the contaminated component.

For the fixed effects $\boldsymbol{\beta}$, we assume a multivariate normal prior with mean $\mathbf{0}$ and covariance matrix $1000 \cdot \mathbf{I}_p$:

$$\boldsymbol{\beta} \sim \text{MVN}(\mathbf{0}, 1000 \cdot \mathbf{I}_p),$$

where \mathbf{I}_p is the $p \times p$ identity matrix.

The error term’s scale parameter σ is modeled using a truncated Student’s t -distribution:

$$\sigma \sim t_+(0, 10, 3),$$

indicating a t -distribution with 3 degrees of freedom, centered at 0, scale 10, and truncated to be positive.

For the parameter γ , we assume a uniform prior over the interval (L_γ, U_γ) :

$$\gamma \sim \text{Uniform}(L_\gamma, U_\gamma).$$

We specify the matrix-generalized half- t (MGH- t) prior distribution of Huang and Wand [16] for the inverse covariance matrix $\boldsymbol{\Sigma}^{-1}$ as a hierarchical mixture of a Wishart distribution and gamma distributions for the diagonal elements of a scale matrix, $\boldsymbol{\Psi}$. Specifically, the diagonal elements of $\boldsymbol{\Psi}$, denoted as ψ_{ii} , follow independent gamma distributions with shape and scale parameters set to 0.5 and $1/50^2$, respectively: $\psi_{ii} \sim \text{Gamma}(0.5, 1/50^2)$. The off-diagonal elements ψ_{ij} for $i \neq j$ are set to zero. The inverse covariance matrix, $\boldsymbol{\Sigma}^{-1}$, follows a Wishart distribution with inverse scale matrix $4\boldsymbol{\Psi}$ and degrees of freedom equal to $d + 1$. This hierarchical formulation corresponds to specifying a half- t prior for the standard deviation terms of $\boldsymbol{\Sigma}$ and a uniform prior, $\text{Uniform}(-1, 1)$, for the correlation parameters.

We assign the contamination weight α a weakly informative Beta(1,9) prior, where the shape parameters 1 and 9 yield a mean of 0.1 and a heavily right-skewed distribution. This choice reflects our expectation that only a small fraction of observations arise from the “contaminated” component while still allowing the data to support larger values of α if necessary. If α grows too large (close to 1), the second (inflated-scale) component ceases to be a “contamination” and instead dominates the mixture. We also fix $\tau_0 = 10$ to provide a sufficiently large “scale” inflation, capturing heavy-tailed behavior without overwhelming the main component. Under these settings, the model remains close to a single-component GAL distribution but retains the flexibility to accommodate outliers through the contamination mixture.

5 Application to HIV dataset

5.1 Nonlinear mixed-effects model

The NLME model we explore is a specific case of the general mixed-effects quantile regression framework introduced in Section 4, tailored for modeling the HIV viral load in the ACTG 315 dataset. In this case, the model is nonlinear, specified as a biphasic (two-phase) exponential decay process that captures both short-term and long-term dynamics of HIV viral load [11]. We model the observed viral load for patient i at time t_{ij} as a combination of two exponential decay processes to explain the biphasic viral decline. The model accounts for both short-term and long-term decay components and includes random effects to capture patient-specific variability.

We model the observed viral load y_{ij} as follows:

$$y_{ij} = \mu_{ij}(p_0) + \varepsilon_{ij}(p_0),$$

where $\mu_{ij}(p_0)$ represents the conditional p_0^{th} quantile of the viral load for patient i at time t_{ij} , and $\varepsilon_{ij}(p_0)$ is an error term such that the p_0^{th} quantile of $\varepsilon_{ij}(p_0)$ is zero. The conditional quantile $\mu_{ij}(p_0)$ is specified as

$$\mu_{ij}(p_0) = \log_{10} \left(P_1 e^{-\lambda_{1i} t_{ij}} + P_2 e^{-\lambda_{2i} t_{ij}} \right),$$

where P_1 and P_2 are the initial viral load components for the two decay phases, and λ_{1i} and λ_{2i} are the corresponding decay rates.

The parameters P_1 , P_2 , λ_{1i} , and λ_{2i} vary across patients according to the following random-effects structure:

$$\begin{aligned} \log(P_1) &= \beta_1 + b_{i1}, \\ \lambda_{1i} &= \beta_2 + b_{i2}, \\ \log(P_2) &= \beta_3 + b_{i3}, \\ \lambda_{2i} &= \beta_4 + \beta_5 \text{CD4}_{ij} + b_{i4}. \end{aligned}$$

Here, β_1 to β_5 are fixed effects, capturing the population-level behavior, while b_{i1} to b_{i4} are random effects that account for patient-specific deviations from the population averages. In this formulation, CD4 count (CD4_{ij}), expressed in units of CD4 cells per 100 mm^3 , is included as a covariate in the long-term decay rate, λ_{2i} , allowing immune status to influence the long-term phase of viral decay.

The random effects vector $\mathbf{b}_i = (b_{i1}, b_{i2}, b_{i3}, b_{i4})'$ is assumed to follow a multivariate normal distribution as in Equation (3).

The NLME model is explored under the three distributional frameworks outlined in Section 4. Hence, each observation y_{ij} is assumed to follow an AL/GAL/cGAL distribution for which the p_0^{th} quantile is centered at $\mu_{ij}(p_0)$.

The choice of $\tau_0 = 10$ for the cGAL model corresponds to 10-fold contamination in the scale parameter σ to account for potential outliers in the viral load data. While we fix τ_0 here for simplicity, one may extend the model to treat τ_0 as another parameter to be estimated. However, this would increase the posterior’s complexity and potentially require careful identifiability considerations.

The priors used in these models will follow those specified earlier in Section 4.

The above NLME model, based on the GAL distribution, was also applied to the ACTG 315 dataset by Yu and Yu [4]. However, they implemented a custom sampler instead of JAGS and adopted different prior specifications. For instance, they employed a Wishart prior for Σ , whereas we use the matrix-generalized half- t distribution.

5.2 Model implementation, adequacy, and comparison

We investigated viral load dynamics at five quantiles, $p_0 = 0.05, 0.25, 0.5, 0.75,$ and 0.95 , to capture both lower and upper extremes along with the median. Clinically, examining the tails (e.g., $p_0 = 0.05$ and $p_0 = 0.95$) helps identify subgroups that either rapidly suppress their viral load or remain persistently high, thereby informing targeted interventions. This broad distribution coverage also allows us to assess both short-term and long-term decay phases across diverse patient trajectories.

All models were implemented and ran in JAGS [9] through the `runjags` package in R [17]. The Bayesian models were executed using Markov chain Monte Carlo (MCMC) sampling, with multiple chains initiated to ensure a thorough exploration of the posterior distribution. Convergence diagnostics were checked for each model using the potential scale reduction factor (\hat{R}), with values below 1.05 indicating acceptable convergence across chains.

For the AL and GAL models, we utilized their mixture representations in Equations (1) and (2) to streamline the MCMC sampling process. In contrast, for the cGAL model, we used the “ones” trick to define its custom likelihood in JAGS. This method uses binary indicator variables that follow a Bernoulli distribution. The probabilities are proportional to the likelihood, scaled by a constant to ensure they remain valid. Compared to the AL and GAL models’ mixture representation, this approach increases computational demands.

In the bi-exponential model, λ_{1i} typically represents the initial, faster decay rate, while λ_{2i} reflects the slower, long-term decay. If λ_{2i} is estimated to be larger than λ_{1i} , their roles reverse, with λ_{2i} governing the initial phase and λ_{1i} the later phase. This reversal also shifts P_{1i} and P_{2i} , associating P_{2i} with the initial decay and P_{1i} with the long-term phase. To prevent this switch, setting initial values so that λ_{1i} is larger than λ_{2i} , along with appropriate values for P_{1i} and P_{2i} , helps preserve the intended structure of the decay phases.

All estimates are based on the posterior median, with 95% highest posterior density (HPD) intervals representing the uncertainty around these estimates.

We present Σ in its inverse form, $\Omega = \Sigma^{-1}$. The entries of Ω are denoted by ω_{ij} , for $1 \leq i, j \leq 4$.

We present quantile-specific predictions for the viral load trajectory over time, setting random effects to zero alongside the fixed-effect parameter estimates and 95% HPD intervals across quantiles under each model. CD4 count is included as a covariate, with predicted values over time based on a random intercept-slope model (intercept of approximately 2.25 and slope of 0.001). Predictions are generated for specific study days in line with the planned schedule of viral load and CD4 cell count measurements, including days 0, 2, 7, 10, 14, 21, 28, and weeks 8, 12, 24, and 48.

The Kullback-Leibler (K-L) divergence is employed to assess the adequacy of the three models to identify influential observations and outliers [18, 19], as outlined in Appendix B.

We conducted a simulation-based residual analysis using the R package DHARMA [20, 21] to evaluate the adequacy of the three models. This method compares the observed data to the posterior predictive distribution, conditioned on the random effects for each observation, thereby generating *scaled residuals* between 0 and 1. We used several tests provided by DHARMA to assess these scaled residuals statistically. The Kolmogorov-Smirnov test evaluated the

uniformity of the residual distribution; a parametric dispersion test checked for overdispersion or underdispersion, and a binomial test flagged observations significantly deviating from model expectations. We report p -values from these tests to determine each model’s adequacy of fit.

The `loo` package [22] in R was used to perform leave-one-out (LOO) cross-validation to compare the models’ predictive performance. To ensure numerical stability in the computation of the GAL and cGAL density functions, especially when dealing with exponentials of large magnitudes, we adopted a numerically stable implementation of the log-density function. The original GAL density function involves exponential and CDF terms that can cause overflow or underflow issues. To mitigate this, we reformulated the density computation to operate primarily on the logarithmic scale.

The R code implementing the methods described in this paper is available on GitHub in the repository Robust-Quantile-cGAL.

In the next sections, we present and discuss the results of these models.

5.3 Model adequacy and comparison

Figure 4, Web Figure 1 (Supplementary Material), and Web Figure 2 show pairwise comparisons of K-L divergence estimates among the models: Figure 4 compares GAL vs. cGAL, Web Figure 1 compares AL vs. cGAL, and Web Figure 2 compares AL vs. GAL. The results indicate that the cGAL consistently achieves the lowest divergence, demonstrating strong robustness to outliers across quantiles. While more resilient than AL, the GAL model still shows higher divergence values than cGAL, and AL exhibits the highest divergence overall, indicating its greater sensitivity to outliers.

The p -values from the standard DHARMA checks on scaled residuals—Kolmogorov–Smirnov for uniformity, a parametric dispersion test, and a binomial outlier test—are presented in Table 1. Generally, the models do not exhibit significant issues, with most p -values remaining above the conventional 5% threshold. However, for $p_0 = 0.75$ and $p_0 = 0.95$, the uniformity test indicates significant deviations, suggesting potential fit problems.

Table 1 presents the LOO information criterion (LOOIC) comparison of the AL, GAL, and cGAL models across five quantiles. The cGAL model consistently shows the lowest LOOIC values, providing the best predictive performance and generalizing more effectively to unseen data. Between AL and GAL, the latter generally outperforms the former, as evidenced by lower LOOIC values in most cases. The enhanced performance of cGAL is consistent with its ability to handle outliers by introducing a second, inflated-scale component, making cGAL the strongest candidate across all studied quantiles.

5.4 Quantile fits

Figure 5 presents the posterior estimates and 95% HPD intervals for the GAL and cGAL models across five quantiles, modeling HIV viral load dynamics over time. In the Supplementary Material, Web Figure 3 provides the same quantile profiles for AL vs. cGAL. Web Figure 4 compares AL vs. GAL.

Figure 6 shows posterior estimates and 95% HPD intervals for β_1 to β_5 across five quantiles, while Web Table 1 summarizes parameter estimates and 95% HPD intervals for all models. From Figure 6, we observe the following:

- As expected, β_1 and β_3 shift upward at higher quantiles since they capture higher intercepts of viral load for more extreme subpopulations.
- No major differences emerged among the models for β_2 and β_5 , indicating that the short-term decay and CD4 effect were relatively stable across quantiles and robust to outliers.
- Estimates for β_4 suggest that the cGAL model generally predicts a faster second-phase decay than do the GAL and AL models, as also illustrated in Figure 5. This can be attributed to the cGAL’s robustness to outliers, particularly in the second phase, where the presence of irregular viral load trajectories influences the GAL and

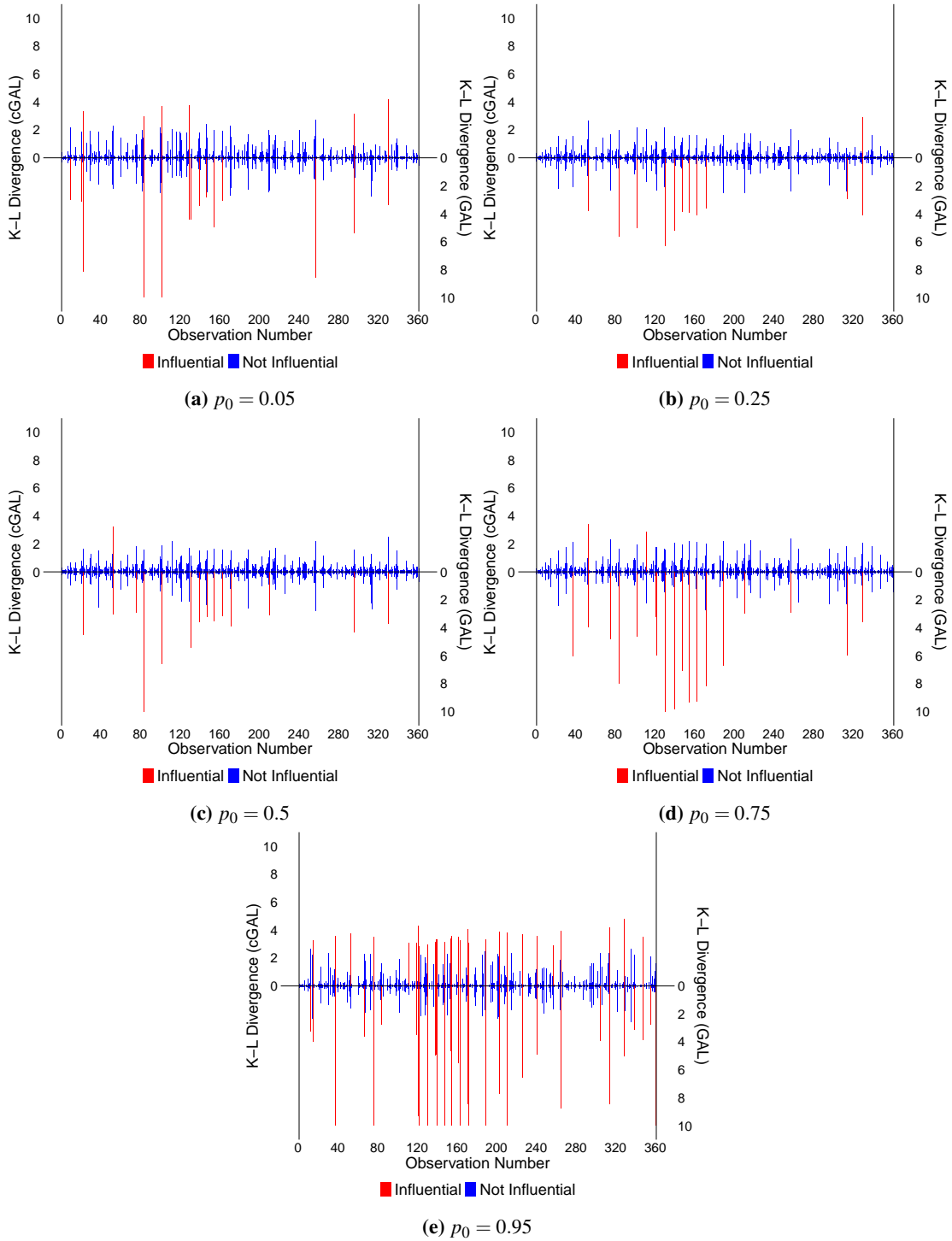


Figure 4: K-L divergence for the GAL and cGAL models across quantiles ($p_0 = 0.05, 0.25, 0.5, 0.75, 0.95$). The K-L divergence, capped at 10, is shown for all observations, with the GAL model on the bottom and the cGAL model on top. Influential observations (see Appendix B for the definition) are highlighted in red, while non-influential ones are in blue. Dual y-axes represent the divergence for each model. Outliers appear to have a much larger impact on the GAL model compared to the cGAL model, indicating that the GAL model is more sensitive to extreme observations.

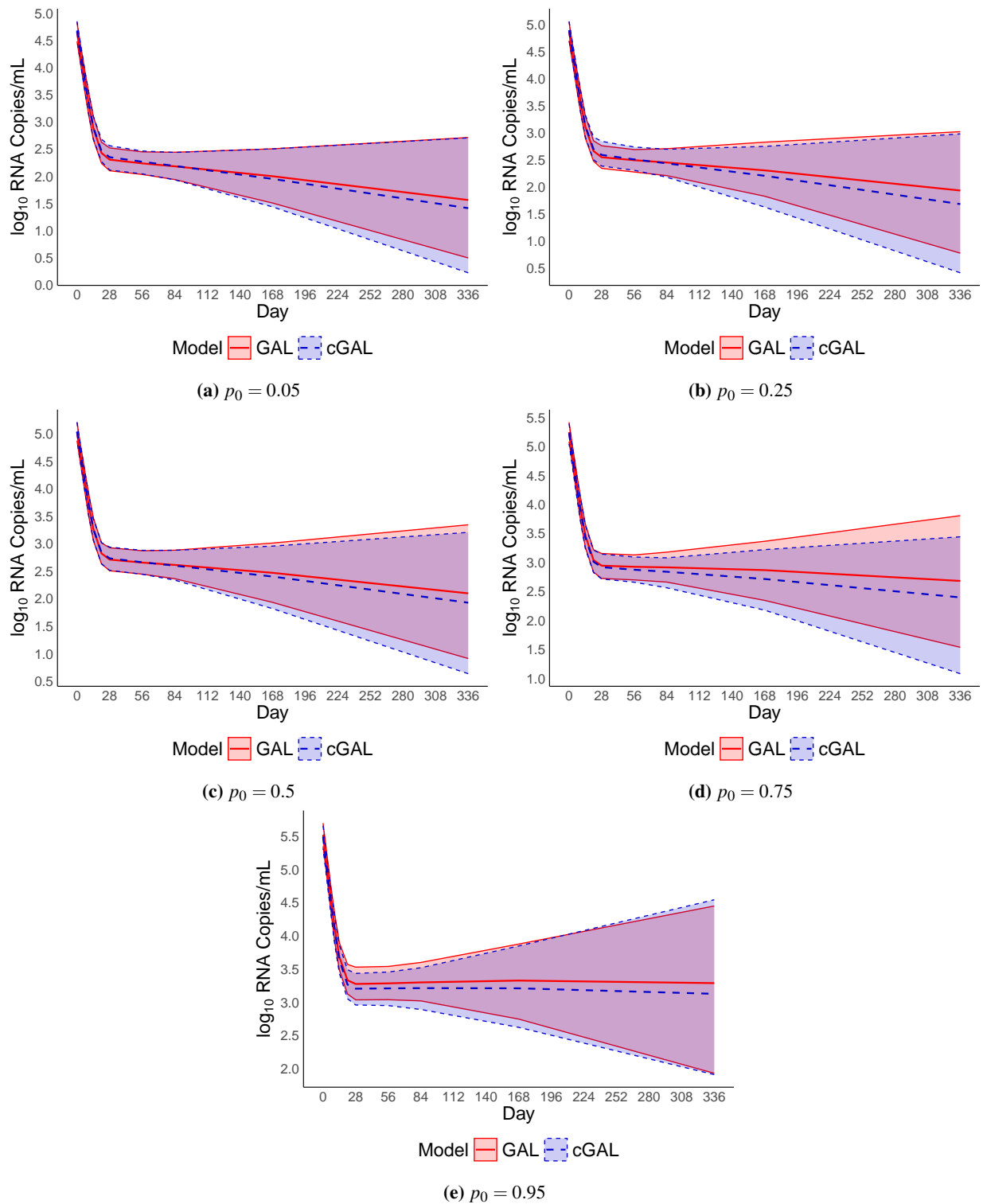


Figure 5: Comparison of quantile profiles for the GAL and cGAL models at five quantiles ($p_0 = 0.05, 0.25, 0.5, 0.75, 0.95$), depicting HIV viral load dynamics over time in the ACTG 315 study. The profiles illustrate the different decay trajectories across the two models, with the GAL model represented by the red solid lines and the cGAL model by the blue dashed lines. The shaded areas represent the 95% HPD intervals around each profile.

Table 1: Comparison of LOOIC between AL, GAL, and cGAL models across quantiles. Additionally, the table includes p -values for the scaled residual diagnostics: a Kolmogorov-Smirnov test (uniformity), a dispersion test (under-/overdispersion), and a binomial test for outliers. In each test, higher p -values (e.g., above 0.05) indicate that the data do not deviate substantially from model assumptions, suggesting a better fit.

Quantile ^a	Model ^b	Uniform ^c	Dispersion ^d	Outliers ^e	LOOIC ^f
0.05	AL	0.052	0.264	>0.999	2890.920
	GAL	0.100	0.220	>0.999	749.032
	cGAL	0.076	0.754	>0.999	643.851
0.25	AL	0.161	0.251	0.165	624.925
	GAL	0.119	0.244	>0.999	655.484
	cGAL	0.085	0.978	>0.999	578.952
0.5	AL	0.093	0.290	0.165	680.793
	GAL	0.107	0.228	>0.999	672.699
	cGAL	0.058	0.820	>0.999	601.527
0.75	AL	0.012	0.474	>0.999	1191.032
	GAL	0.056	0.288	0.165	818.534
	cGAL	0.029	0.835	>0.999	640.377
0.95	AL	0.029	0.550	>0.999	6010.133
	GAL	0.026	0.412	>0.999	1356.416
	cGAL	0.022	0.712	>0.999	923.316

^a Quantile level being modeled.

^b AL (asymmetric Laplace), GAL (generalized asymmetric Laplace), cGAL (contaminated GAL).

^c p -value from the Kolmogorov-Smirnov test (uniformity).

^d p -value from the dispersion test (under-/overdispersion).

^e p -value from the binomial outlier test.

^f LOOIC (leave-one-out information criterion).

AL models, pulling their estimates upward and slowing the decay (see Figure 1). In contrast, the cGAL model is less affected by these outliers, resulting in a more accurate representation of long-term viral load dynamics.

The parameter estimates align with our model comparison results, confirming that the cGAL's robust handling of outliers yields steeper long-term decay rates.

6 Simulation study

6.1 Model performance

A simulation study was conducted to assess the performance of the cGAL model within the proposed NLME quantile regression framework in Section 5.1. Data were generated under a two-phase viral load model for $N = 15$ subjects, each observed at $J_i = 9$ time points. Specifically, the model assumed:

$$y_{ij} = \log_{10}(\exp(\beta_1 + b_{i1} - (\beta_2 + b_{i2})t_{ij}) + \exp(\beta_3 - \beta_4 t_{ij})),$$

where y_{ij} denotes the outcome at the j^{th} measurement for cluster i , and $t_{ij} = j - 1$ so that t_{ij} ranges from 0 to 8. The parameters β_1 and β_2 were the main focus (representing the short-term viral load component), while β_3 and β_4 were fixed at their true values and were not estimated.

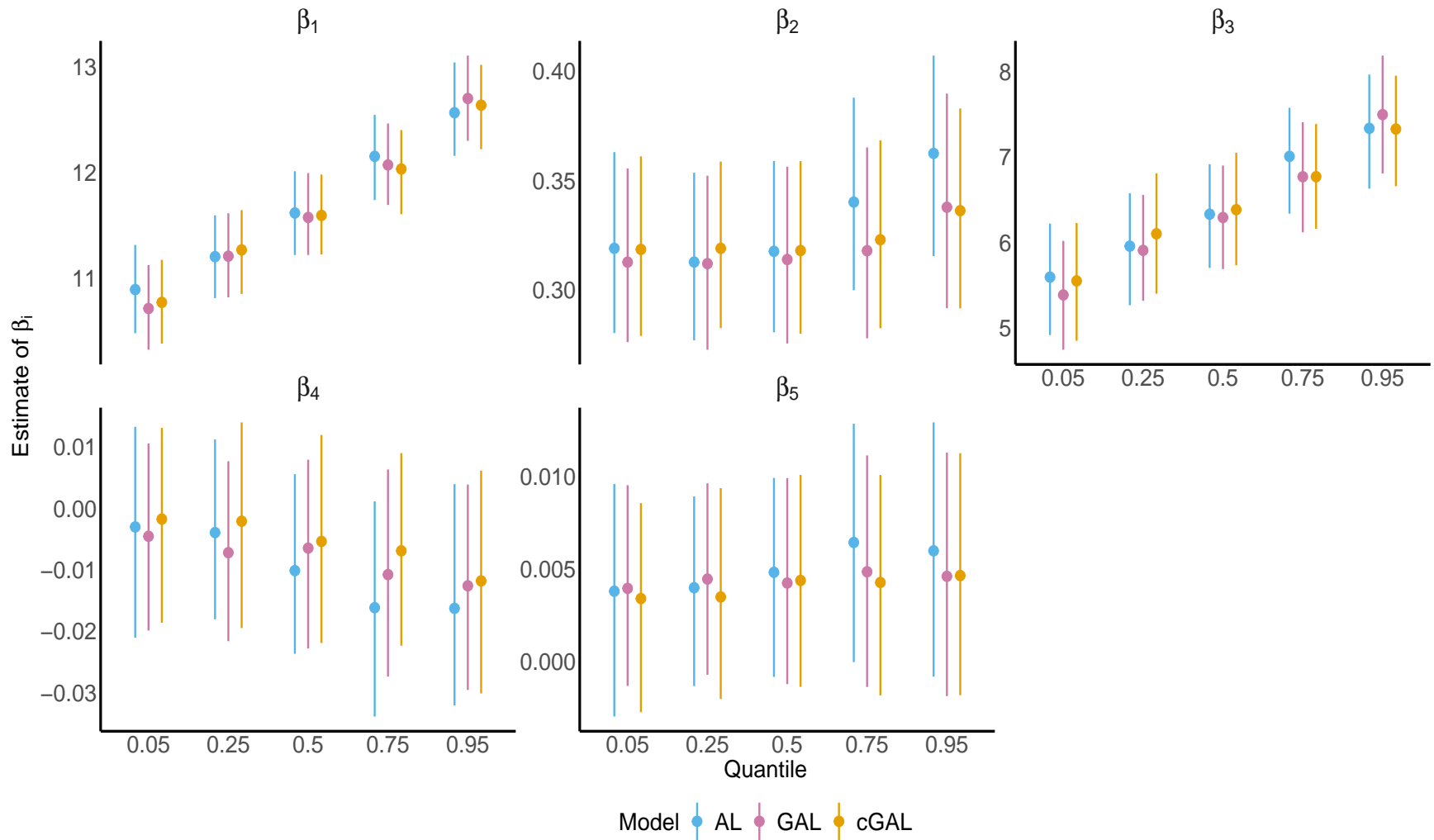


Figure 6: Posterior estimates and 95% HPD intervals for the fixed effect parameters across quantiles $p_0 = 0.05, 0.25, 0.5, 0.75, 0.95$. The estimates are shown for three models: AL (blue), GAL (purple), and cGAL (orange) applied within an NLME framework to the HIV viral load in the ACTG 315 dataset. Here, β_1 and β_3 represent the initial viral load components for the short- and long-term decay phases, respectively. The short-term decay rate is captured by β_2 . The long-term decay rate is represented by β_4 and incorporates CD4 as a covariate, with β_5 as its regression coefficient.

Random effects $\mathbf{b}_i = (b_{i1}, b_{i2})'$ were drawn from a bivariate normal distribution with zero mean and covariance matrix:

$$\boldsymbol{\Sigma} = \begin{pmatrix} 0.95^2 & 0.05 \times 0.95 \times 0.95 \\ 0.05 \times 0.95 \times 0.95 & 0.95^2 \end{pmatrix}.$$

The parameter values were set to $\beta_1 = 11.5$, $\beta_2 = 5.5$, $\beta_3 = 3.5$, $\beta_4 = 0.05$, $\sigma = 0.2$, and $\tau_0 = 10$. A shape parameter $\gamma = -0.3$ governed skewness.

We report

$$\boldsymbol{\Sigma}^{-1} = \begin{pmatrix} \omega_{11} & \omega_{12} \\ \omega_{12} & \omega_{22} \end{pmatrix}$$

here to remain consistent with the approach used in the application section (see Section 5.2).

We assume a Uniform(0, 1) prior for α , a more noninformative choice than the beta-distributed prior used in the application, which places greater mass on smaller values of α .

Four scenarios were created by varying the contamination proportion α (either 0.001 or 0.05) and the target quantile p_0 (either 0.50 or 0.85). In each scenario, 300 datasets were generated. Model fitting and parameter inference were performed using the same NLME framework but substituting the appropriate likelihood (AL, GAL, or cGAL). Primary outcomes included bias and coverage probabilities of 95% HPD intervals.

The model performance results are presented in Web Table 2 of the Supplementary Material. Coverage probabilities for the model parameters range from acceptable (meeting nominal targets) to conservative, with none being overly lenient. However, higher contamination levels lead to increased bias in β_2 , and the variance components also exhibit substantial bias, consistent with the findings by Burger et al. [23] for the covariance matrix under the MGH- t prior distribution.

6.2 Robustness under data contamination

We conducted a data contamination simulation study to evaluate the robustness of the GAL model relative to the cGAL model, using the same scenarios described in Section 6.1 while sampling from the cGAL model. We report bias, coverage probabilities of 95% HPD intervals, root mean square error (RMSE), and HPD interval width for β_1 and β_2 .

The results of the data contamination study are presented in Web Table 3. Under minimal contamination ($\alpha = 0.1\%$), both GAL and cGAL perform similarly. However, when 5% contamination is introduced ($\alpha = 5\%$), both the RMSE and HPD interval length for β_2 are substantially larger for the GAL model than for the cGAL model. These findings suggest that the cGAL model is more robust to outliers than the GAL model.

7 Discussion

In this paper, we developed a robust mixed-effects quantile regression framework for modeling HIV viral load decay, comparing the AL, GAL, and cGAL distributions in an NLME setting. Our results indicate that the cGAL distribution, through its improved treatment of outliers in viral load data, more reliably captures the dynamics of HIV progression.

An important practical consideration is that the cGAL model, while more robust to outliers than its AL and GAL counterparts, is computationally more demanding. Unlike AL and GAL, which have convenient mixture representations facilitating sampling, the cGAL distribution requires a custom likelihood formulation (via the ‘‘ones trick’’ in JAGS), substantially increasing runtime. This trade-off may be critical in large-scale studies or real-time clinical settings where computational efficiency is paramount. Nonetheless, the computational overhead may be justified when data contain influential outliers, given the cGAL’s superior robustness and improved predictive performance in our results.

We introduced τ_0 as a scale inflation factor for the contaminated component of the cGAL distribution, fixing it to a relatively large value (in our case, $\tau_0 = 10$) to ensure sufficient coverage for potential heavy-tailed behavior. Although choosing a fixed value can work well in practice, especially if we suspect pronounced outliers, estimating τ_0 from the data could present greater flexibility. In such an extended model, both the contamination proportion α and scale factor τ_0 would be unknown parameters. This may present identifiability challenges, such as distinguishing whether extreme observations arise from a heavily scaled component or a small fraction of contamination. However, it arguably provides a clearer perspective on outlier behavior.

Although we treated observed viral load data in a straightforward manner, future research may account for left-censored observations below the limit of quantification (LLOQ), which is common in HIV studies. In principle, the NLME model could handle this by treating sub-threshold observations as censored. However, implementing censoring under the GAL or cGAL distributions is nontrivial due to the lack of closed-form CDFs. A specialized sampling scheme or additional numerical integration might be required to accommodate censoring within the robust quantile framework. Similarly, incorporating measurement error in the CD4 covariate could refine the modeling of its effect on long-term viral decay [24]. Presently, we assume that CD4 was measured without error, but realistic clinical data often include substantial variability. Approaches such as Bayesian measurement-error models or joint modeling of CD4 and viral load could better characterize how immune status covaries with viral trajectory.

Across the two contamination levels and target quantiles considered, the cGAL model’s coverage often exceeds the 95% target, indicating a conservative stance rather than an overly lenient one. The data contamination study further shows that the GAL is considerably affected by moderate contamination compared to the cGAL, particularly regarding RMSE and HPD interval width.

In summary, the cGAL-based NLME quantile model constitutes a robust alternative to classical AL or GAL approaches by eliminating the need for explicit outlier identification and deletion. It exhibits stronger resistance to the effects of outliers while yielding more reliable model parameter estimates.

Appendix

A L-statistic-based kurtosis

The L-statistic-based kurtosis is computed separately for a sorted sample’s left and right tails to capture the distribution’s tail behavior around the median. Given an ordered sample $\{X_{(1)}, X_{(2)}, \dots, X_{(n)}\}$, the sample median $F_n^{-1}(0.5)$ is defined as $X_{(\frac{n}{2})}$ for an even sample size n . The left-side kurtosis $\phi_{n,L}$ is then calculated as:

$$\phi_{n,L} = \frac{\frac{2}{n} \sum_{i=1}^{n/2} \binom{4i-2}{n} X_{(i)}}{F_n^{-1}(0.5) - \frac{2}{n} \sum_{i=1}^{n/2} X_{(i)}}.$$

Similarly, the right-side kurtosis $\phi_{n,D}$ is computed as:

$$\phi_{n,D} = \frac{\frac{2}{n} \sum_{i=n/2+1}^n \binom{4i-2}{n} X_{(i)}}{\frac{2}{n} \sum_{i=n/2+1}^n X_{(i)} - F_n^{-1}(0.5)}.$$

B Kullback-Leibler divergence

To evaluate the influence of individual data points on the model, we use LOO to measure model adequacy following the approach detailed by Wang and Luo [18]. Specifically, we compute the K-L divergence, quantifying the difference between model fits when a particular observation is included versus excluded.

Let $\boldsymbol{\eta}$ denote the collection of parameters. For the AL model, $\boldsymbol{\eta} = (\boldsymbol{\beta}', \sigma)'$ includes the fixed effects vector $\boldsymbol{\beta}$ and scale parameter σ . For the GAL model, $\boldsymbol{\eta} = (\boldsymbol{\beta}', \sigma, \gamma)'$, where γ is the skewness parameter. In the cGAL model, $\boldsymbol{\eta} = (\boldsymbol{\beta}', \sigma, \gamma, \alpha)'$, where α is the contamination parameter. Let Θ represent the complete set of model parameters, including both fixed and random effects.

Let $\boldsymbol{\eta}^{(k)}$ and $\mathbf{b}_i^{(k)}$ represent the k^{th} posterior sample of parameters $\boldsymbol{\eta}$ and random effects \mathbf{b}_i , respectively, for $k = 1, \dots, K$. The vector \mathbf{y} consists of all observations y_{ij} for subjects $i = 1, \dots, N$ and measurements $j = 1, \dots, J_i$. The posterior distribution of the parameters Θ given the full dataset is denoted by $P(\Theta | \mathbf{y})$, while $P(\Theta | \mathbf{y}_{[ij]})$ refers to the posterior distribution of Θ after element-wise exclusion of the single observation y_{ij} . The Monte Carlo estimate of the K-L divergence between the posterior distributions under regression model R is computed as:

$$\begin{aligned} \text{KL}_R \left(P(\Theta | \mathbf{y}), P(\Theta | \mathbf{y}_{[ij]}) \right) &= \log \left\{ \frac{1}{K} \sum_{k=1}^K \left[P(y_{ij} | \boldsymbol{\eta}^{(k)}, \mathbf{b}_i^{(k)}) \right]^{-1} \right\} \\ &\quad + \frac{1}{K} \sum_{k=1}^K \log \left[P(y_{ij} | \boldsymbol{\eta}^{(k)}, \mathbf{b}_i^{(k)}) \right]. \end{aligned}$$

This K-L divergence is calculated for each observation y_{ij} to evaluate its potential influence under regression model R , identifying observations that may substantially impact the parameter estimates. Following Tomazella et al. [19], we flag observation y_{ij} as influential ("outlier") if it meets the following criterion:

$$0.5 \left(1 + \sqrt{1 - \exp \left[-2 \text{KL}_R \left(P(\Theta | \mathbf{y}), P(\Theta | \mathbf{y}_{[ij]}) \right) \right]} \right) \geq 0.999.$$

Supplementary information

Supplementary material for this paper is available online. Example code for the model application is available on Robust-Quantile-cGAL on GitHub.

Acknowledgements

This work is based on the research supported by the National Research Foundation (NRF) of South Africa (Grant number 132383). Opinions expressed and conclusions arrived at are those of the authors and are not necessarily to be attributed to the NRF.

Declaration of conflicting interests

The authors declare no conflict of interest.

References

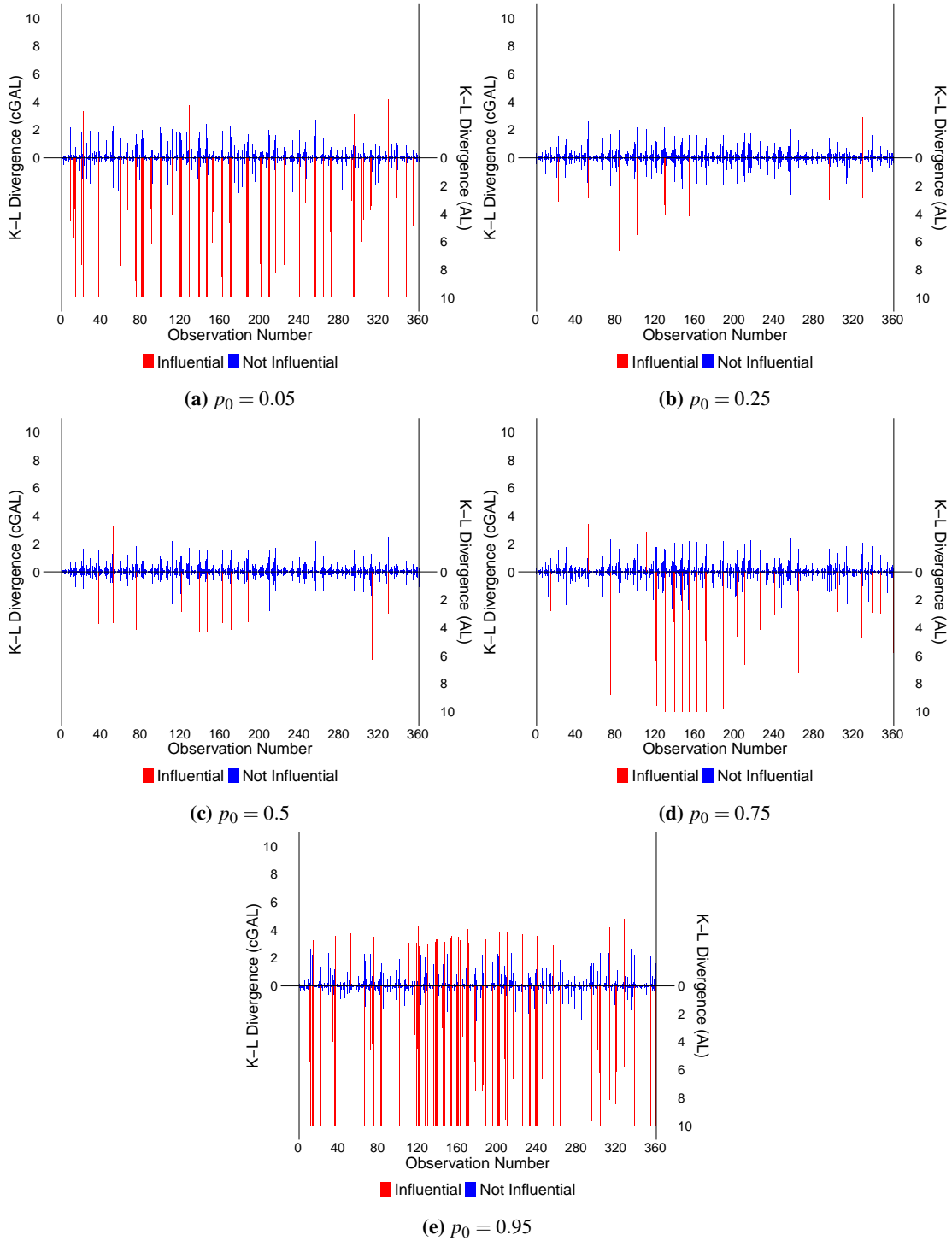
- [1] R. Koenker and K. F. Hallock. Quantile regression. *The Journal of Economic Perspectives*, 15(4):143–156, 2001.
- [2] M. Geraci and M. Bottai. Quantile regression for longitudinal data using the asymmetric Laplace distribution. *Biostatistics*, 8(1):140–154, 2007.
- [3] Y. Yan and A. Kottas. A new family of error distributions for Bayesian quantile regression, 2017. arXiv preprint arXiv:1701.05666.
- [4] H. Yu and L. Yu. Flexible Bayesian quantile regression for nonlinear mixed effects models based on the generalized asymmetric Laplace distribution. *Journal of Statistical Computation and Simulation*, 93(15):2725–2750, 2023.

- [5] R. Barata. *Flexible dynamic quantile linear models*. Ph.D. dissertation, University of California, Santa Cruz, 2021.
- [6] A. J. Florez, I. van Keilegom, G. Molenberghs, and A. Verhasselt. Quantile regression for longitudinal data via the multivariate generalized hyperbolic distribution. *Statistical Modelling*, 22(6):566–584, 2022.
- [7] N. Wichitaksorn, S. B. Choy, and R. Gerlach. A generalized class of skew distributions and associated robust quantile regression models. *Canadian Journal of Statistics*, 42(4):579–596, 2014.
- [8] M. Bernardi, M. Bottone, and L. Petrella. Bayesian quantile regression using the skew exponential power distribution. *Computational Statistics & Data Analysis*, 126:92–111, 2018.
- [9] M. Plummer. JAGS: A program for analysis of Bayesian graphical models using Gibbs sampling. In *Proceedings of the 3rd International Workshop on Distributed Statistical Computing*, pages 1–10. Vienna, Austria, 2003.
- [10] S. E. Morris, L. Dziobek-Garrett, and A. Yates. *ushr: understanding suppression of HIV*, 2020. R package version 0.2.3.
- [11] A. S. Perelson, A. U. Neumann, M. Markowitz, J. M. Leonard, and D. D. Ho. HIV-1 dynamics in vivo: virion clearance rate, infected cell life-span, and viral generation time. *Science*, 271(5255):1582–1586, 1996.
- [12] P. W. Nelson and A. S. Perelson. Mathematical analysis of delay differential equation models of HIV-1 infection. *Mathematical Biosciences*, 179(1):73–94, 2002.
- [13] J. W. Tukey. A survey of sampling from contaminated distributions. In *Contributions to Probability and Statistics*, pages 448–485. Stanford University Press, 1960.
- [14] P. J. Huber. Robust estimation of a location parameter. In S. Kotz and N. L. Johnson, editors, *Breakthroughs in Statistics*. Springer Series in Statistics, Springer, New York, NY, 1992.
- [15] A. M. Fiori and D. Beltrami. Right and left kurtosis measures: large sample estimation and an application to financial returns. *Stat*, 3(1):95–108, 2014.
- [16] A. Huang and M. P. Wand. Simple marginally noninformative prior distributions for covariance matrices. *Bayesian Analysis*, 8(2):439–452. DOI: 10.1214/13-BA815, 2013.
- [17] M. J. Denwood. runjags: An R package providing interface utilities, model templates, parallel computing methods and additional distributions for MCMC models in JAGS. *Journal of Statistical Software*, 71(9):1–25, 2016.
- [18] J. Wang and S. Luo. Augmented Beta rectangular regression models: A Bayesian perspective. *Biometrical Journal*, 58(1):206–221, 2016.
- [19] V. L. D. Tomazella, S. R. Jesus, A. B. Gazon, F. Louzada, S. Nadarajah, D. C. Nascimento, F. A. Rodrigues, and P. L. Ramos. Bayesian reference analysis for the generalized normal linear regression model. *Symmetry*, 13(5):856, 2021.
- [20] F. Hartig. *DHARMA: residual diagnostics for hierarchical (multi-level/mixed) regression models*, 2021. R package version 0.4.4.
- [21] F. Hartig. DHARMA: residual diagnostics for hierarchical (multi-level/mixed) regression models. <https://cran.r-project.org/web/packages/DHARMA/vignettes/DHARMA.html>, September 2021.
- [22] A. Vehtari, J. Gabry, M. Magnusson, Y. Yao, P.-C. Bürkner, T. Paananen, and A. Gelman. loo: Efficient leave-one-out cross-validation and WAIC for Bayesian models, 2024. R package version 2.8.0.
- [23] D. A. Burger, R. Schall, J. T. Ferreira, and D.-G. Chen. A robust Bayesian mixed effects approach for zero inflated and highly skewed longitudinal count data emanating from the zero inflated discrete Weibull distribution. *Statistics in Medicine*, 39(9):1275–1291., 2020.
- [24] L. Wu. A joint model for nonlinear mixed-effects models with censoring and covariates measured with error, with application to AIDS studies. *Journal of the American Statistical Association*, 97(460):955–964, 2002.

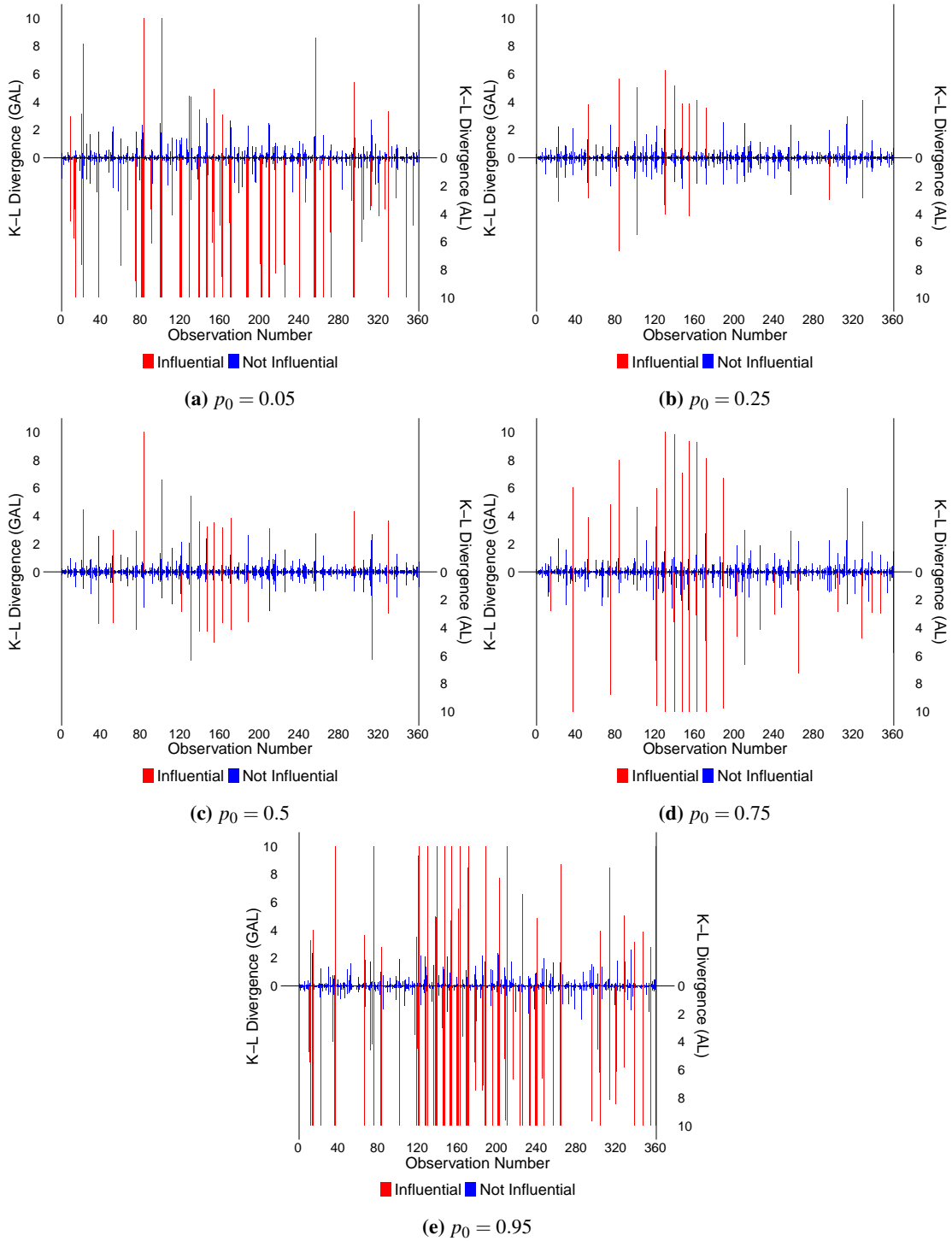
A robust mixed-effects quantile regression model using generalized Laplace mixtures to handle outliers and skewness

Divan A. Burger, Sean van der Merwe, and Emmanuel Lesaffre

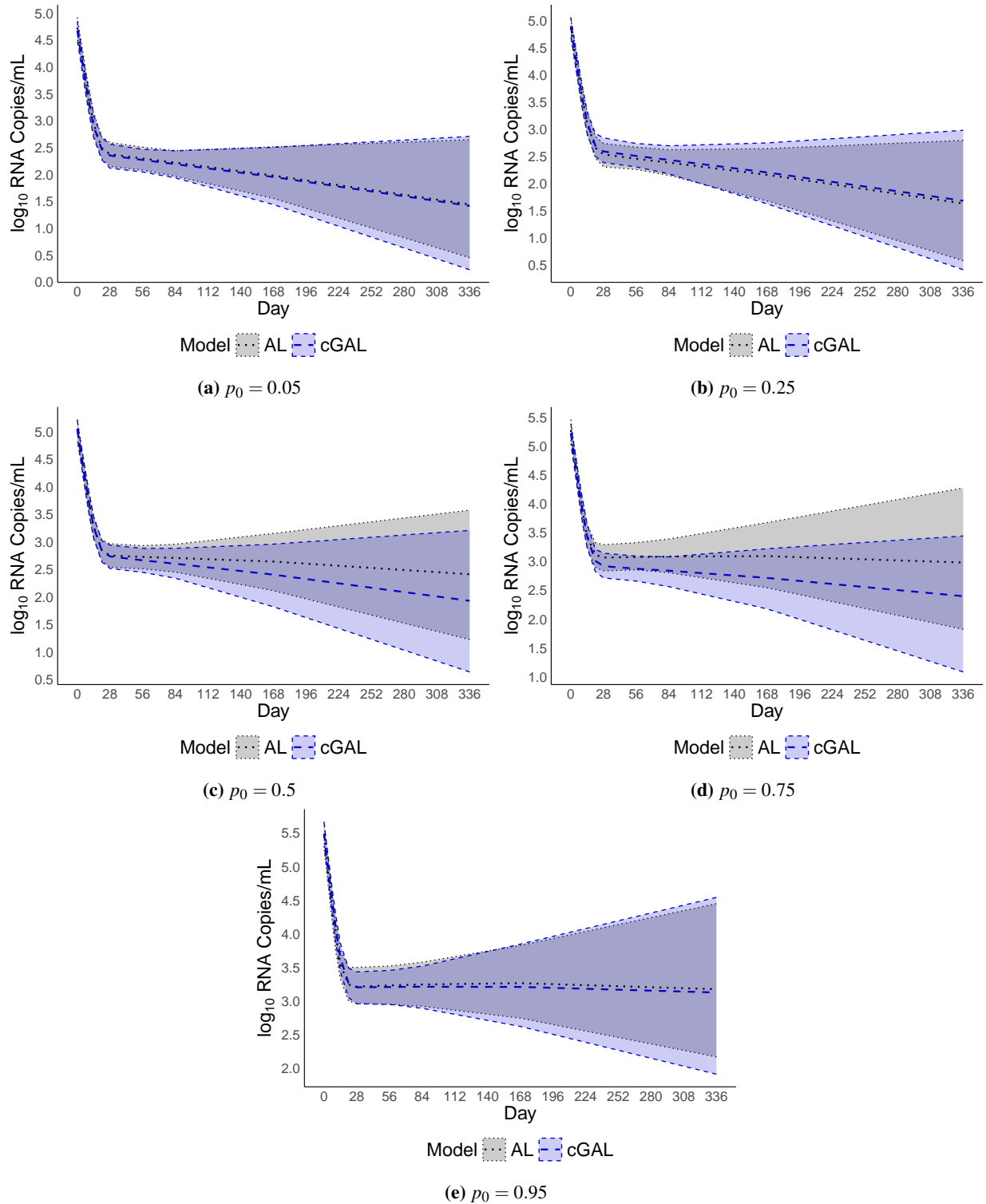
Supporting Information



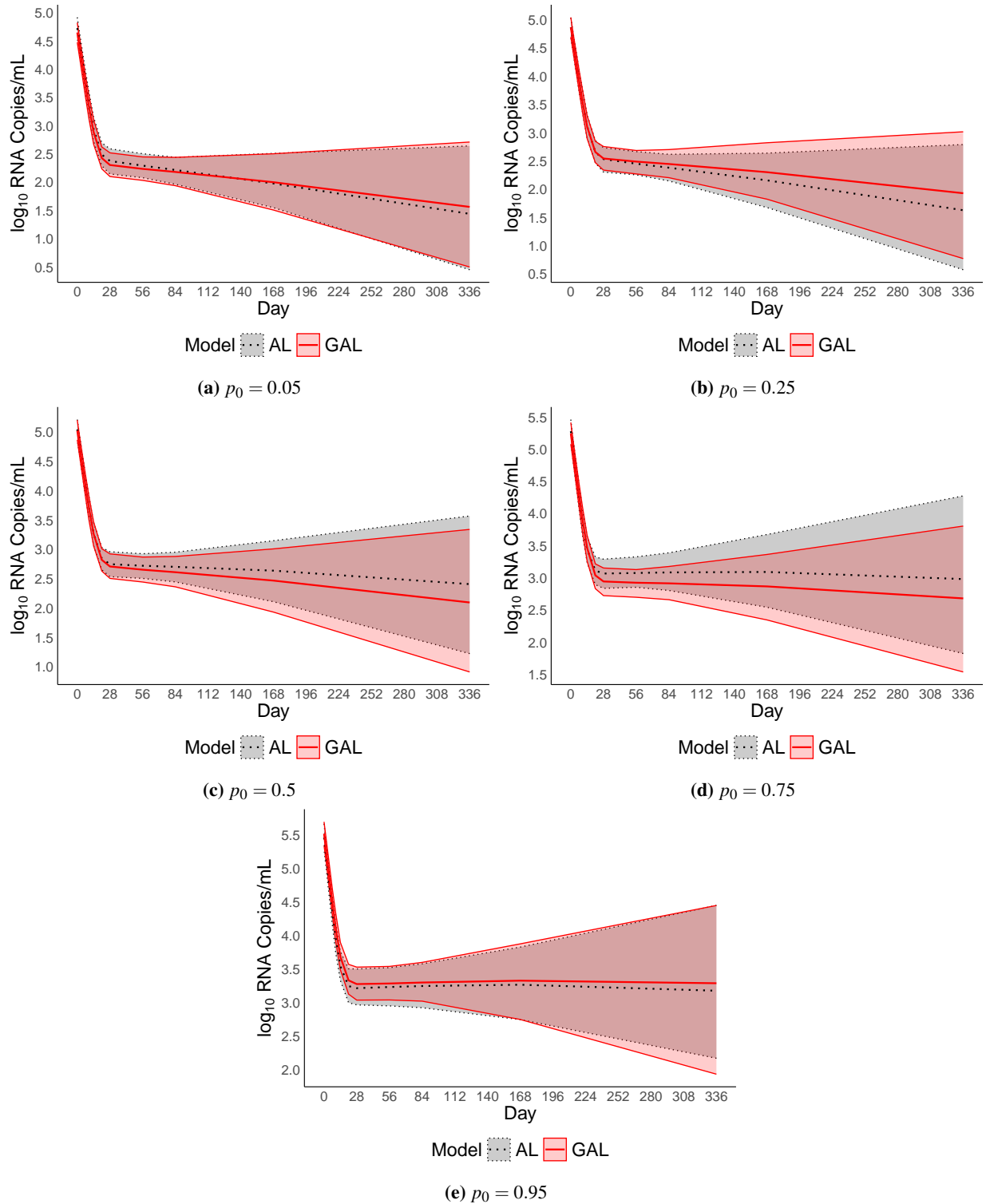
WEB FIGURE 1: K-L divergence for the AL and cGAL models across quantiles ($p_0 = 0.05, 0.25, 0.5, 0.75, 0.95$). The K-L divergence, capped at 10, is shown for all observations, with the AL model on the bottom and the cGAL model on top. Influential observations (see Appendix B for the definition) are highlighted in red, while non-influential ones are in blue. Dual y-axes represent the divergence for each model. Outliers appear to have a much larger impact under the AL model compared to the cGAL model, indicating that the AL model is more sensitive to extreme observations.



WEB FIGURE 2: K-L divergence for the AL and GAL models across quantiles ($p_0 = 0.05, 0.25, 0.5, 0.75, 0.95$). The K-L divergence, capped at 10, is shown for all observations, with the AL model on the bottom and the GAL model on top. Influential observations (see Appendix B for the definition) are highlighted in red, while non-influential ones are in blue. Dual y-axes represent the divergence for each model. Outliers generally have a larger impact under the AL model compared to the GAL model, suggesting that the AL model is more sensitive to extreme observations.



WEB FIGURE 3: Comparison of quantile profiles for the AL and cGAL models at five quantiles ($p_0 = 0.05, 0.25, 0.5, 0.75, 0.95$), depicting HIV viral load dynamics over time in the ACTG 315 study. The profiles illustrate the different decay trajectories across the two models, with the AL model represented by the black dotted lines and the cGAL model by the blue dashed lines. The shaded areas represent the 95% HPD intervals around each profile.



WEB FIGURE 4: Comparison of quantile profiles for the AL and GAL models at five quantiles ($p_0 = 0.05, 0.25, 0.5, 0.75, 0.95$), depicting HIV viral load dynamics over time in the ACTG 315 study. The profiles illustrate the different decay trajectories across the two models, with the AL model represented by the black dotted lines and the GAL model by the red solid lines. The shaded areas represent the 95% HPD intervals around each profile.

WEB TABLE 1: Posterior summaries for each quantile level under the AL, GAL, and cGAL models. Columns report each parameter's posterior estimate (Est.) and 95% HPD interval. Results for higher quantiles continue on subsequent pages.

Quantile ^a	Parameter	Model ^b								
		AL			GAL			cGAL		
		Est.	95% HPD		Est.	95% HPD		Est.	95% HPD	
0.05	β_1	10.888	[10.473;	11.311]	10.708	[10.317;	11.120]	10.766	[10.375;	11.169]
	β_2	0.319	[0.280;	0.363]	0.313	[0.276;	0.355]	0.318	[0.279;	0.361]
	β_3	5.590	[4.912;	6.217]	5.382	[4.740;	6.015]	5.546	[4.845;	6.224]
	β_4	-0.003	[-0.021;	0.013]	-0.005	[-0.020;	0.011]	-0.002	[-0.019;	0.013]
	β_5	0.004	[-0.003;	0.010]	0.004	[-0.001;	0.010]	0.003	[-0.003;	0.009]
	σ	0.021	[0.018;	0.024]	0.067	[0.055;	0.078]	0.057	[0.036;	0.071]
	γ				2.847	[1.968;	3.824]	4.058	[2.225;	6.975]
	α							0.018	[0.002;	0.038]
	ω_{11}	0.929	[0.452;	1.600]	1.139	[0.515;	2.210]	1.094	[0.484;	1.987]
	ω_{21}	2.042	[-2.583;	8.240]	3.393	[-3.734;	15.857]	2.958	[-3.758;	13.770]
	ω_{22}	126.647	[45.138;	273.301]	182.982	[41.391;	495.406]	175.010	[57.743;	442.609]
	ω_{31}	-0.374	[-0.807;	-0.056]	-0.469	[-1.102;	-0.092]	-0.465	[-1.045;	-0.087]
	ω_{32}	-0.377	[-5.359;	4.413]	-1.594	[-10.095;	5.187]	-1.945	[-10.519;	3.920]
	ω_{33}	0.647	[0.329;	1.079]	0.728	[0.346;	1.262]	0.719	[0.333;	1.231]
	ω_{41}	14.600	[-8.951;	44.343]	15.825	[-15.627;	51.615]	13.007	[-12.288;	42.097]
	ω_{42}	-106.832	[-534.535;	273.684]	-165.956	[-823.793;	408.179]	-176.357	[-774.993;	198.428]
	ω_{43}	-24.531	[-51.701;	-4.272]	-25.121	[-51.457;	-2.802]	-22.975	[-45.799;	-4.021]
	ω_{44}	3550.850	[1563.010;	7617.490]	3775.830	[1668.130;	7478.400]	3171.280	[1607.770;	5613.480]

Continued on next page

(continued)

Quantile ^a	Parameter	Model ^b								
		AL			GAL			cGAL		
		Est.	95% HPD		Est.	95% HPD		Est.	95% HPD	
0.25	β_1	11.200	[10.806;	11.592]	11.204	[10.813;	11.612]	11.264	[10.846;	11.642]
	β_2	0.313	[0.277;	0.354]	0.312	[0.273;	0.352]	0.319	[0.282;	0.359]
	β_3	5.953	[5.261;	6.573]	5.904	[5.313;	6.553]	6.098	[5.396;	6.806]
	β_4	-0.004	[-0.018;	0.011]	-0.007	[-0.022;	0.008]	-0.002	[-0.020;	0.014]
	β_5	0.004	[-0.001;	0.009]	0.004	[-0.001;	0.010]	0.003	[-0.002;	0.009]
	σ	0.093	[0.081;	0.107]	0.111	[0.095;	0.131]	0.097	[0.041;	0.121]
	γ				0.473	[0.063;	0.833]	0.745	[0.129;	2.113]
	α							0.022	[0.002;	0.051]
	ω_{11}	1.112	[0.506;	2.040]	1.174	[0.532;	2.177]	1.115	[0.543;	2.030]
	ω_{21}	2.896	[-4.712;	16.280]	3.385	[-5.005;	19.242]	2.688	[-6.698;	16.022]
	ω_{22}	206.009	[61.341;	610.099]	218.843	[57.340;	719.243]	213.755	[61.322;	782.779]
	ω_{31}	-0.447	[-1.019;	-0.043]	-0.487	[-1.108;	-0.079]	-0.465	[-1.085;	-0.087]
	ω_{32}	-1.145	[-11.137;	7.147]	-1.869	[-14.249;	5.966]	-1.524	[-12.826;	10.053]
	ω_{33}	0.729	[0.339;	1.250]	0.753	[0.344;	1.353]	0.755	[0.330;	1.328]
	ω_{41}	17.577	[-10.986;	50.696]	18.502	[-11.716;	52.047]	12.994	[-16.221;	40.612]
	ω_{42}	-181.731	[-935.112;	286.107]	-194.774	[-1036.640;	330.180]	-222.341	[-1062.980;	360.416]
	ω_{43}	-27.220	[-55.447;	-6.385]	-26.756	[-55.040;	-5.211]	-24.384	[-50.962;	-3.354]
	ω_{44}	3734.935	[1592.020;	7133.150]	3600.175	[1598.020;	6855.200]	3220.385	[1497.850;	6166.040]

Continued on next page

(continued)

Quantile ^a	Parameter	Model ^b								
		AL			GAL			cGAL		
		Est.	95% HPD		Est.	95% HPD		Est.	95% HPD	
0.5	β_1	11.614	[11.216;	12.011]	11.572	[11.216;	11.993]	11.591	[11.220;	11.980]
	β_2	0.318	[0.281;	0.359]	0.314	[0.275;	0.356]	0.318	[0.280;	0.359]
	β_3	6.327	[5.698;	6.913]	6.289	[5.684;	6.897]	6.380	[5.729;	7.047]
	β_4	-0.010	[-0.024;	0.006]	-0.006	[-0.023;	0.008]	-0.005	[-0.022;	0.012]
	β_5	0.005	[-0.001;	0.010]	0.004	[-0.001;	0.010]	0.004	[-0.001;	0.010]
	σ	0.126	[0.109;	0.144]	0.112	[0.020;	0.137]	0.102	[0.039;	0.129]
	γ				-0.326	[-0.983;	-0.057]	-0.242	[-0.836;	0.097]
	α							0.018	[0.001;	0.045]
	ω_{11}	1.201	[0.559;	2.336]	1.180	[0.504;	2.259]	1.112	[0.543;	2.066]
	ω_{21}	3.293	[-5.487;	17.590]	3.526	[-4.655;	18.509]	2.735	[-6.302;	16.953]
	ω_{22}	206.829	[64.149;	684.648]	218.613	[61.656;	657.225]	214.907	[58.781;	738.424]
	ω_{31}	-0.487	[-1.140;	-0.071]	-0.491	[-1.147;	-0.058]	-0.465	[-1.055;	-0.069]
	ω_{32}	-1.710	[-13.728;	7.355]	-1.855	[-12.912;	6.737]	-1.912	[-13.632;	9.802]
	ω_{33}	0.775	[0.376;	1.435]	0.768	[0.357;	1.382]	0.744	[0.340;	1.314]
	ω_{41}	18.944	[-10.219;	51.400]	17.725	[-13.623;	50.222]	15.522	[-10.741;	46.174]
	ω_{42}	-165.159	[-949.283;	332.340]	-202.437	[-989.776;	346.832]	-218.613	[-1114.230;	273.108]
	ω_{43}	-26.966	[-56.662;	-6.934]	-27.142	[-55.074;	-5.559]	-24.462	[-49.770;	-4.232]
	ω_{44}	3289.345	[1451.350;	5738.650]	3568.830	[1648.540;	6723.000]	3166.495	[1543.930;	5895.370]

Continued on next page

(continued)

Quantile ^a	Parameter	Model ^b								
		AL			GAL			cGAL		
		Est.	95% HPD		Est.	95% HPD		Est.	95% HPD	
0.75	β_1	12.152	[11.737;	12.546]	12.071	[11.691;	12.464]	12.032	[11.603;	12.402]
	β_2	0.340	[0.300;	0.388]	0.318	[0.278;	0.365]	0.323	[0.282;	0.368]
	β_3	7.005	[6.334;	7.574]	6.766	[6.116;	7.404]	6.767	[6.157;	7.384]
	β_4	-0.016	[-0.034;	0.001]	-0.011	[-0.027;	0.006]	-0.007	[-0.022;	0.009]
	β_5	0.006	[0.000;	0.013]	0.005	[-0.001;	0.011]	0.004	[-0.002;	0.010]
	σ	0.095	[0.081;	0.109]	0.104	[0.072;	0.130]	0.085	[0.043;	0.113]
	γ				-1.240	[-1.804;	-0.741]	-1.408	[-2.100;	-0.854]
	α							0.015	[0.001;	0.035]
	ω_{11}	1.170	[0.503;	2.123]	1.232	[0.539;	2.447]	1.136	[0.544;	2.105]
	ω_{21}	1.698	[-9.533;	24.553]	3.447	[-4.343;	17.750]	2.972	[-3.983;	14.787]
	ω_{22}	156.002	[30.900;	2301.640]	193.226	[48.892;	570.078]	186.693	[59.594;	472.967]
	ω_{31}	-0.446	[-1.040;	-0.029]	-0.498	[-1.261;	-0.066]	-0.462	[-1.064;	-0.075]
	ω_{32}	-0.271	[-9.905;	24.276]	-2.358	[-12.522;	7.086]	-2.335	[-10.780;	4.892]
	ω_{33}	0.733	[0.336;	1.416]	0.770	[0.380;	1.468]	0.736	[0.367;	1.339]
	ω_{41}	18.636	[-3.281;	44.942]	18.428	[-8.155;	53.426]	14.099	[-12.459;	42.389]
	ω_{42}	-37.728	[-730.643;	916.398]	-159.418	[-857.598;	280.474]	-204.434	[-837.495;	225.430]
	ω_{43}	-18.554	[-39.966;	-0.101]	-25.136	[-51.927;	-4.386]	-21.977	[-46.403;	-3.833]
	ω_{44}	2311.940	[1084.790;	3975.270]	3201.290	[1538.090;	5923.810]	2989.335	[1392.050;	5168.770]

Continued on next page

(continued)

Quantile ^a	Parameter	Model ^b								
		AL			GAL			cGAL		
		Est.	95% HPD		Est.	95% HPD		Est.	95% HPD	
0.95	β_1	12.566	[12.157;	13.044]	12.701	[12.300;	13.108]	12.638	[12.221;	13.021]
	β_2	0.362	[0.315;	0.407]	0.338	[0.292;	0.390]	0.336	[0.291;	0.383]
	β_3	7.333	[6.626;	7.963]	7.494	[6.803;	8.185]	7.325	[6.656;	7.951]
	β_4	-0.016	[-0.032;	0.004]	-0.013	[-0.030;	0.004]	-0.012	[-0.030;	0.006]
	β_5	0.006	[-0.001;	0.013]	0.005	[-0.002;	0.011]	0.005	[-0.002;	0.011]
	σ	0.020	[0.018;	0.023]	0.070	[0.059;	0.080]	0.060	[0.042;	0.075]
	γ				-3.734	[-4.940;	-2.627]	-4.568	[-6.571;	-2.968]
	α						0.012	[0.000;	0.028]	
	ω_{11}	0.839	[0.441;	1.318]	1.096	[0.501;	2.071]	1.044	[0.519;	1.945]
	ω_{21}	-0.404	[-4.923;	4.207]	1.508	[-6.642;	15.837]	1.484	[-4.387;	9.463]
	ω_{22}	94.944	[28.917;	246.147]	132.469	[25.499;	888.207]	128.435	[37.715;	312.930]
	ω_{31}	-0.289	[-0.623;	-0.025]	-0.404	[-0.941;	-0.013]	-0.389	[-0.913;	-0.037]
	ω_{32}	-0.165	[-4.611;	5.048]	-1.314	[-11.223;	11.052]	-1.491	[-8.969;	3.656]
	ω_{33}	0.548	[0.268;	0.935]	0.676	[0.283;	1.267]	0.658	[0.337;	1.181]
	ω_{41}	12.566	[-0.376;	28.142]	16.897	[-4.247;	43.502]	16.197	[-3.971;	43.321]
	ω_{42}	-50.011	[-294.766;	170.620]	-17.611	[-524.265;	456.264]	-78.953	[-497.389;	238.236]
	ω_{43}	-13.750	[-26.763;	-1.535]	-18.478	[-38.568;	-2.496]	-18.885	[-39.459;	-2.917]
	ω_{44}	1910.535	[996.911;	3076.930]	2276.790	[1068.020;	3898.490]	2522.015	[1207.850;	4309.600]

^a Quantile level being modeled.

^b AL (asymmetric Laplace), GAL (generalized asymmetric Laplace), cGAL (contaminated GAL).

WEB TABLE 2: Model performance characteristics for the cGAL model under various scenarios. Columns “ p_0 ” and “ α ” correspond to the target quantile and contamination level, respectively. The column “True” denotes the true parameter value, “Bias” is the mean difference between the estimated and true values, and “CP” represents the coverage probability of the 95% HPD intervals.

p_0^a	α^b	Parameter	True ^c	Bias ^d	CP ^e
0.50	0.001	β_1	11.500	0.023	0.970
		β_2	5.500	0.311	0.980
		σ	0.200	-0.024	0.940
		γ	-0.300	-0.060	0.973
		α	0.001	0.016	0.980
		ω_{11}	1.111	1.348	0.983
		ω_{12}	-0.056	0.001	1.000
		ω_{22}	1.111	0.622	0.997
		0.50	0.050	β_1	11.500
β_2	5.500			0.570	0.973
σ	0.200			-0.019	0.957
γ	-0.300			-0.016	0.973
α	0.050			0.015	0.930
ω_{11}	1.111			1.247	0.977
ω_{12}	-0.056			0.012	1.000
ω_{22}	1.111			0.529	0.993
0.85	0.001			β_1	11.500
		β_2	5.500	0.614	0.997
		σ	0.200	-0.001	0.987
		γ	-0.300	-0.232	0.963
		α	0.001	0.030	0.977
		ω_{11}	1.111	0.991	0.983
		ω_{12}	-0.056	0.001	1.000
		ω_{22}	1.111	0.414	0.993
		0.85	0.050	β_1	11.500
β_2	5.500			1.088	0.980
σ	0.200			0.004	0.983
γ	-0.300			-0.294	0.947
α	0.050			0.015	0.950
ω_{11}	1.111			1.000	0.983
ω_{12}	-0.056			0.003	1.000
ω_{22}	1.111			0.272	0.993

^a p_0 is the target quantile level.

^b α is the contamination level.

^c “True” denotes the true parameter value.

^d “Bias” is the mean difference between the estimated and true values.

^e “CP” is the coverage probability of the 95% HPD intervals.

WEB TABLE 3: Model performance characteristics for GAL and cGAL fixed effects parameters under various scenarios. Columns “ p_0 ” and “ α ” correspond to the target quantile and contamination level, respectively. The column “True” denotes the true parameter value, “Bias” is the mean difference between the estimated and true values, “RMSE” is the root mean square error, “CP” is the coverage probability of the 95% HPD intervals, and “HPD Len.” is the mean width of the HPD interval.

p_0^a	α^b	Model ^c	Parameter	True ^d	Bias ^e	RMSE ^f	CP ^g	HPD Len. ^h
0.50	0.001	GAL	β_1	11.500	0.031	0.420	0.967	1.822
			β_2	5.500	0.319	0.857	0.970	6.238
0.50	0.001	cGAL	β_1	11.500	0.023	0.416	0.970	1.813
			β_2	5.500	0.311	0.846	0.980	6.058
0.50	0.050	GAL	β_1	11.500	0.072	0.483	0.973	2.159
			β_2	5.500	1.141	3.441	0.987	14.892
0.50	0.050	cGAL	β_1	11.500	0.005	0.459	0.967	1.939
			β_2	5.500	0.570	2.068	0.973	7.811
0.85	0.001	GAL	β_1	11.500	0.004	0.494	0.993	2.413
			β_2	5.500	0.604	2.047	0.997	7.065
0.85	0.001	cGAL	β_1	11.500	-0.019	0.498	0.993	2.411
			β_2	5.500	0.614	2.068	0.997	7.108
0.85	0.050	GAL	β_1	11.500	0.219	0.605	0.963	2.745
			β_2	5.500	1.252	3.552	0.977	11.498
0.85	0.050	cGAL	β_1	11.500	-0.015	0.522	0.970	2.486
			β_2	5.500	1.088	3.179	0.980	9.722

^a p_0 is the target quantile level.

^b α is the contamination level.

^c GAL (generalized asymmetric Laplace), cGAL (contaminated GAL).

^d “True” denotes the true parameter value.

^e “Bias” is the mean difference between the estimated and true values.

^f “RMSE” is the root mean square error.

^g “CP” is the coverage probability of the 95% HPD intervals.

^h “HPD Len.” is the mean width of the HPD interval.